Mon. Not. R. astr. Soc. (1986) **219,** 75–88

Spiral shocks on a Roche lobe overflow in a semi-detached binary system

K. Sawada *Aircraft Engineering Division, Kawasaki Heavy Industries Ltd, Kakamigahara 504, Japan*

T. Matsuda and I. Hachisu *Department of Aeronautical Engineering, Kyoto University, Kyoto 606, Japan*

Accepted 1985 September 5. Received 1985 August 19; in original form 1985 April 23

Summary. Two-dimensional hydrodynamic calculations of a Roche lobe overflow in a semi-detached binary system with a mass ratio of unity are carried out. The region of the computation covers both a mass-losing star filling its critical Roche lobe and a mass-accreting compact star. Gas ejected from the mass-losing star with specified energy flows through the L1 point to form an elephant trunk and an accretion ring. It is found that spiral-shaped shocks are formed on the accretion ring. It is suggested that the gas in the accretion ring loses angular momentum at the shocks and spirals in towards the compact star even without viscosity.

1 Introduction

A gas flow in a semi-detached binary system is a very important phenomenon in binary studies. We can classify two types of such a flow, i.e. a Roche lobe overflow and a stellar wind. The flow patterns of both types have been studied numerically by many workers.

Early contributions were calculations of free-particle trajectories. The free-particle approximation, however, is irrelevant, because the mean free path of the gas is much shorter than the typical length scale. A hydrodynamic treatment is therefore essential.

Prendergast (1960) was the first to compute the hydrodynamics in a close binary system. The two stars were assumed to be point masses, which did not eject or absorb gas, in his calculation. Biermann (1971) computed the stellar wind using the method of characteristics. His method, however, cannot treat subsonic flow regions, and possible shock waves were not obtained. Prendergast & Taam (1974) considered the case in which the mass-accreting star was rather large. Their method of solution was the beam scheme.

Sorenson, Matsuda & Sakurai (1975) and Sorensen (1976) computed the Roche lobe overflow and the stellar wind using a FLIC-type finite difference method. Flannery (1975) computed the flow around a compact mass-accreting star and found a hotspot. However, Lin & Pringle (1976) and Hensler (1982) used particle schemes to simulate the flow.

A possible drawback in almost all the studies mentioned above is the existence of a large amount of artificial (or numerical) viscosity, which is necessary to stabilize computations in most numerical schemes. However, it has a tendency to smear out the fine structure of the flow. One may argue that such numerical viscosity simulates a turbulent viscosity, which is a necessary ingredient to transfer the angular momentum of gas in an accretion disc outwards.

Before constructing a very realistic model of the gas flow in a semi-detached binary system, it would be necessary to perform precise hydrodynamic calculations of the gas flow under simplified assumptions. In the present paper we perform two-dimensional hydrodynamic calculations of the flow of inviscid adiabatic gas using a modern technique of computational fluid dynamics.

We use the Osher upwind scheme (Osher & Chakravarthy 1983; Chakravarthy & Osher 1983) which can compute very strong shock waves without an explicit artificial viscosity. Although the absence of the artificial viscosity does not necessarily mean the absence of numerical diffusivity, the effect is minimized by applying a second-order-accurate scheme and a very fine grid system.

The flow patterns that we obtain in this work agree generally with the results of Sorensen *et al.* (1975). However, there is an important difference: we found that there are spiral-shaped shock waves on the accretion disc (ring). These shocks were probably smeared out by excessive artificial and/or numerical viscosity in earlier work.

They are produced by the non-axisymmetric gravitational potential near the compact mass-accreting star, which is caused by the tidal effect due to the mass-losing star. Gas loses angular momentum at the shock and can spiral in towards the compact star. The angular momentum is transferred from the gas to the orbital motion by gravitational interaction. Therefore, an interesting possibility arises: viscosity may not be necessary for the gas to be accreted into the compact star.

2 The model

We consider a semi-detached binary system with a mass ratio of unity. We restrict our computation to a thin disc on the equatorial plane. Fig. 1 shows the Roche potential seen on the equatorial plane. In the potential there are five neutral points, at which the effects of gravity and the centrifugal force cancel, and they are denoted by L1–L5. Although these points are generally

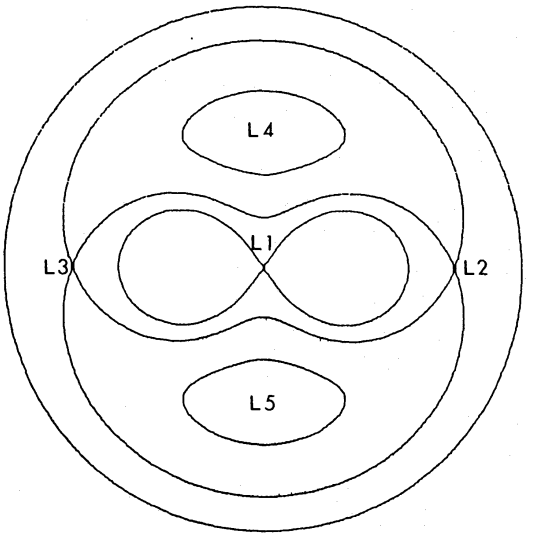

Figure 1. The Roche potential seen on equatorial plane. L1–L5 represent so-called Lagrangian points.

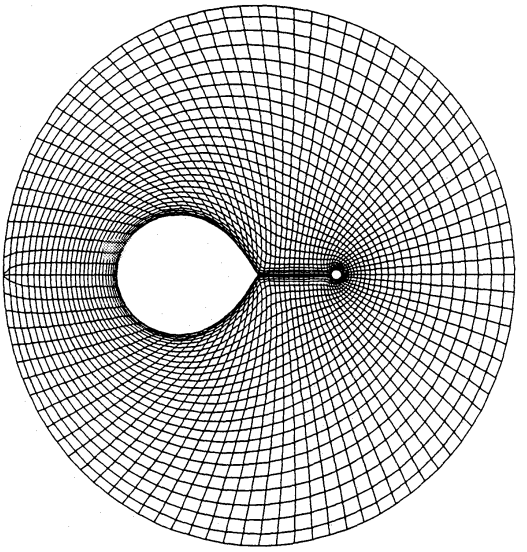

Figure 2. The generalized curvilinear coordinate used here. The mesh size is 28×95.

referred to as Lagrangian points, L1–L3 were first noted by Euler (Kozai 1984, private communication).

The mass-losing star fills up its own critical Roche lobe. If the mass-accreting star is an ordinary main-sequence star, it is possible to construct a mesh covering the surface of the star. Since we are interested in a binary system containing a compact star such as a white dwarf, a neutron star or a black hole, it is not practical to cover the surface (or the event horizon) of the star by the computational mesh. Therefore we replace the mass-accreting star by a small central hole on which a free boundary condition is imposed. We shall call this hole a compact star or a mass-accreting star hereafter.

The gas is assumed to be ejected perpendicularly from the surface of the mass-losing star. The density ϱ_0, the velocity $(u_0^2+v_0^2)^{1/2}$ and the sound speed c_0 of the gas just inside the surface of the star are specified. The density and the velocity are kept constant in each case, while the sound speed is a parameter to be varied. We consider only the case of subsonic mass ejection in the present work.

The actual boundary condition at the surface of the star is computed by solving a Riemann problem between the state just inside the star and that just outside. Therefore the mass loss rate is not fixed but is regulated through the pressure of gas at the bottom of the atmosphere. All gas arriving on the surface of the mass-accreting star is assumed to be absorbed.

We assume the whole process to be adiabatic in the sense that the gas has a constant ratio of specific heats. Entropy increases only at the shocks, if the numerical computation is strictly accurate. We neglect possible heating of gas by the illumination from the compact star. However, in order to simulate the effect of cooling, we consider the case with a lower ratio of the specific heats.

As was discussed in Section 1, we neglect viscosity in the computation. Therefore we solve the Euler equation rather than the Navier–Stokes equation. An explicit artificial viscosity is not included in our numerical scheme, but a truncation error inherent in the scheme plays a similar role.

Gas is assumed to be confined in a plane with a constant thickness. This simplification is justified if we restrict our attention to the region very close to the equatorial plane.

On this two-dimensional plane a body-fitted coordinate shown in Fig. 2 is constructed. The number of meshes is 28 for the radial direction and 95 for the azimuthal direction except for one

case in which the number of meshes in the radial direction is doubled. This computational domain is wide enough to treat possible mass loss from the system and is fine enough to compute a complex flow around the compact star.

The basic equations are made dimensionless by using the separation A of the two stars as the length scale, the reciprocal of the angular speed of revolution (Ω^{-1}) as the time-scale and the density under the surface of the mass-losing star as the density scale. The velocity scale is $A\Omega$.

In the present study, ϱ_0 is fixed to be unit, $(u_0^2+v_0^2)^{1/2}$ is 0.0125 and c_0 is a free parameter to be varied. Three cases, $c_0=0.05$, 0.15 and 0.5, are computed. The ratio γ of specific heats is set to be 5/3 except for the case $c_0=0.15$, for which a value of $\gamma=1.2$ is also used.

At the surface of the compact star and the outer numerical boundary, physical variables are linearly extrapolated from the interior points. These quantities are used to give the boundary conditions by solving the Riemann problems (see the Appendix for details).

We try to obtain a possible steady state by following the time evolution of the system starting at some initial condition. Since with the Eulerian method it is difficult to treat a vacuum state, we assume the existence of traces of gas everywhere except inside the stars in the initial stage. The density of this ambient gas is set to be so low (10^{-5}) that it will not have any effect on the subsequent evolution. An advantage of using the Osher scheme is the ability to handle such a sharp density contrast stably.

The ambient gas is assumed to be at rest in the rotational frame at the initial epoch. The temperature of the ambient gas may be chosen arbitrarily, but it is chosen to be 10 times higher than that of the gas ejected from the star. Since the entropies of these two gases are very different, it is easy to identify the origin of the gases at a later epoch.

Numerical calculations were performed using the Fujitsu VP100 vector processor; the maximum speed is 260 Mflops. We could achieve only 70–80 Mflops because the Osher scheme is very complicated. This value is still satisfactory compared with, for example, the 2.5 Mflops attainable on an IBM-3081K scalar computer. One time-step takes 0.08 s, and we computed for 1–1.5 hr to obtain one model. Such a long computation time is necessary because of the Courant condition imposed by the very fine mesh near the compact star.

3 Result

3.1 THE CASE OF $c_0=0.15$ AND $\gamma=5/3$

Fig. 3(a, b and c) shows the density distribution, the Mach number distribution with velocity vectors, and the distribution of the entropy define as $\log(p/\varrho^\gamma)$, respectively, for a (quasi) steady state in which c_0 and γ are chosen as 0.15 and 5/3 respectively. This is our standard model.

We start the computation from the initial homogeneous static state without an accretion disc and follow the evolution for about four revolution periods. The density distribution near the compact star reaches a steady state within one revolution period, while it takes two to three revolution periods for the outer part. It should be noted that the steady state is not steady in a strict sense, but oscillates. The density pattern and the shock position change with time periodically, although the general pattern is the same.

As can be seen in Fig. 3(a and b), gas ejected from the mass-losing star mainly goes through the L1 point to form an 'elephant trunk'. Gas cannot hit the compact star directly because of the Coriolis force. The main part of the gas turns around the compact star and forms an accretion disc. Since the density near the compact star is lower than that at the outer part of the accretion disc, it may be appropriate to call it an accretion ring. The cause of the density diminution around the compact star is that the gas is transferred towards the compact star quickly and swallowed by it.

Why does it happen without viscosity? It is partly because of the numerical viscosity and partly because of the spiral shocks on the accretion disc (ring).

Let us discuss the numerical viscosity first. Although our method of calculation does not need an explicit artificial viscosity, none the less the truncation error works as a sort of viscosity. Since our method is of second-order accuracy, the numerical Reynolds' number is of the order of $(r/\delta r)^2$, where δr is a mesh spacing, and is typically about 100 near our compact star. Because of this numerical viscosity the angular momentum of the gas is transferred outwards and the gas spirals in towards the compact star. The effect of the numerical viscosity can be reduced by increasing the number of meshes. This will be discussed later.

Now let us discuss the spiral shocks. As can be seen in Fig. 3(b), gas leaving the L1 point, which works as a Laval nozzle, soon becomes supersonic. If the gravitational potential were axisymmetric about the compact star, the velocity would be kept supersonic and shocks would not occur. However, because of the presence of the companion star, the gravitational potential about the compact star is not axisymmetric.

It has been shown in the study of barred spiral galaxies (Sorensen, Matsuda & Fujimoto 1976; Sanders & Huntley 1976; see Matsuda 1981 for other references) that a supersonic flow in a non-axisymmetric potential results in spiral-shaped shocks. Spiral shocks in barred galaxies do not extend to the centre, because the gas velocity becomes zero at the centre. However, in the present binary shocks, the gas velocity increases towards the compact star, although non-axisymmetry diminishes towards the compact star. Therefore shocks reach the inner boundary.

Gas hitting the shock is decelerated, and the velocity component normal to the shock becomes subsonic. The velocity vectors are deflected towards the compact star. Gas loses angular momentum and spirals in towards the compact star. The angular momentum of the gas is given to the orbital motion through gravitational interaction.

The radius of our 'compact star' is about $0.03A$ and may not be small enough as a realistic compact star. It would be interesting to see how deep the present shocks penetrate towards the real compact star when the radius of the inner boundary is reduced. This will be studied in future work.

The gas is accelerated again by the gravitational force, and another shock is formed at the opposite side of the former shock. It is sometimes argued that a gas stream leaving the L1 point hits the accretion disc to form a shock observed as a hotspot (Flannery 1975). Such a picture is not confirmed in the present calculations. Our secondary shock is not formed by the collision of two streams but because of the non-axisymmetric nature of the potential. The collision of two streams would form a pair of shocks in these streams.

There is some observational evidence suggesting the existence of shocks. In order to explain the light curves of low-mass X-ray binaries, particularly X1822−301 and X2129+47, White & Mason (1984) suggested a model in which the height of the accretion disc varies azimuthally. Since our calculations are concerned only with the flow on the equatorial plane, it is not possible to give the height variation. Nevertheless, it is expected that the thickness of the disc increases suddenly behind the shock, if γ is larger than unity. We plan to extend the present computation to three dimensions.

Observing Fig. 3(b), one can find another shock at the leading hemisphere of the mass-losing star. There is also an indication of a shock at the leading hemisphere of the compact star. This type of shock also is produced because of non-axisymmetry of the gravitational potential. Sawada, Hachisu & Matsuda (1984) found this type of shock in the simulation of the gas outflow from a contact binary system. Gas leaving the binary system obtains angular momentum through collision with these shocks.

Fig. 3(c) shows the entropy distribution. Gas with low entropy is ejected from the mass-losing star into an ambient gas with high entropy. The interface between these two gases is clearly observed. The entropy of the gas around the compact star become high because of shock heating.

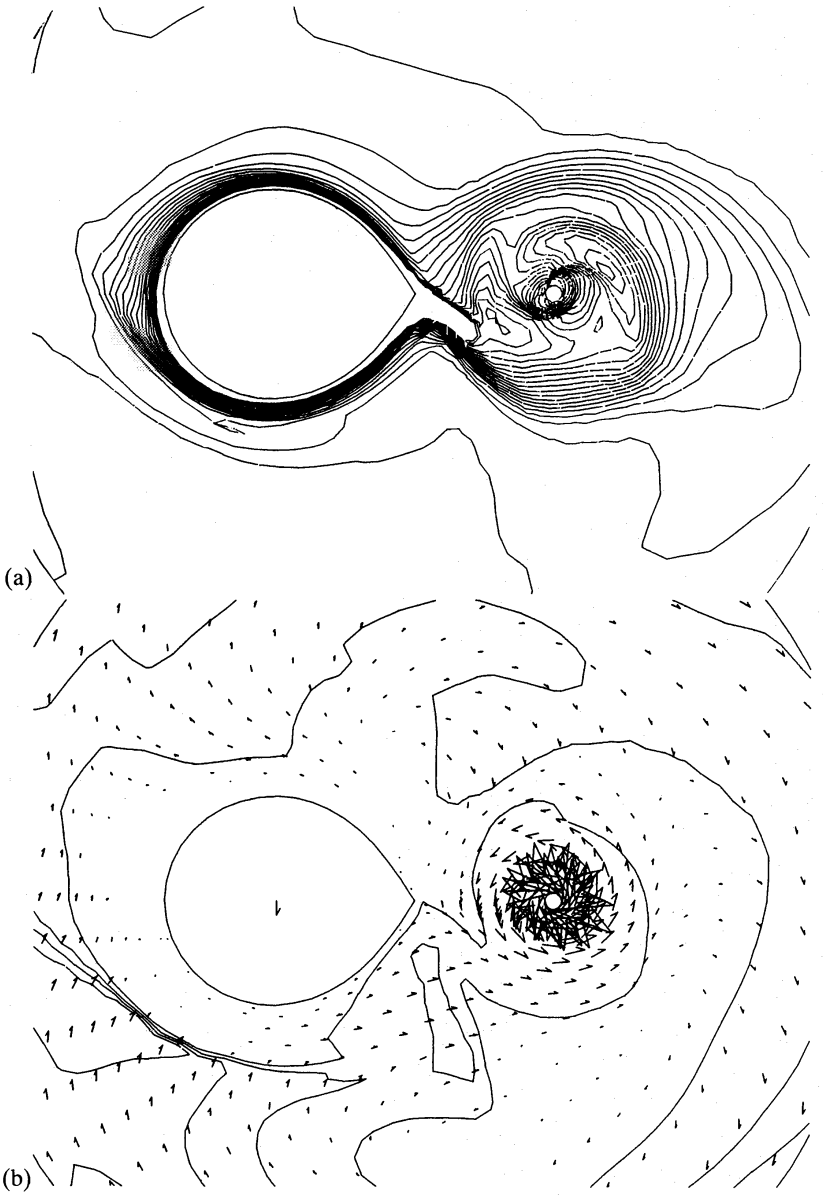

Figure 3. (a) Density contours of the standard model ($c_0=0.15$ and $\gamma=5/3$). The density range from 0.002 to 0.1 is divided by 20 lines with an equal increment. The system rotates counterclockwise. (b) Mach number contours ranging from 1 to 4. Velocity vectors seen from the rotational frame are also shown. A unit vector is given at the centre of the mass-losing star. (c) Entropy contours showing that gas with low entropy is emitted into an ambient gas with high entropy.

A fair amount of gas is absorbed by the compact star, but some gas escapes from the system through the L2 point. Very little gas escapes through the L3 point. This result does not agree with that of Hensler (1982), who argued that the disc was inflated beyond the Roche area and particles were distributed homogeneously in the outer part of the computational region. Our result supports the results by Sorensen *et al.* (1975) and Lin & Pringle (1976).

3.2 THE CASE OF A LOWER SPECIFIC HEAT RATIO

In the above example, gas is assumed to be adiabatic except on shock heating. In a realistic accretion disc, an effect of cooling cannot be ignored. In order to simulate the cooling effect, a case of lower γ is examined. We computed three cases: $\gamma=4/3$, 1.2 and 1.1. The last case was not

(c)

Figure 3 – *continued*

successful because of numerical instability. Therefore we discuss the case $\gamma=1.2$ in this section. The density pattern is shown in Fig. 4.

In a gas with lower γ shocks are much stronger. The maximum Mach number in the elephant trunk is about 2 for $\gamma=5/3$, while it is 10 for $\gamma=1.2$. The density behind the shock is higher, and the temperature behind the shock is lower, compared with the case $\gamma=5/3$. The fraction of the gas accreted on to the compact star is much larger than the high γ case, and this will be discussed later.

3.3 THE CASE OF COOLER GAS EMITTED FROM THE STAR

The sound speed of gas at the surface of the mass-losing star in the above two examples is 0.15 in our dimensionless units. In order to estimate the temperature, let us assume the typical velocity

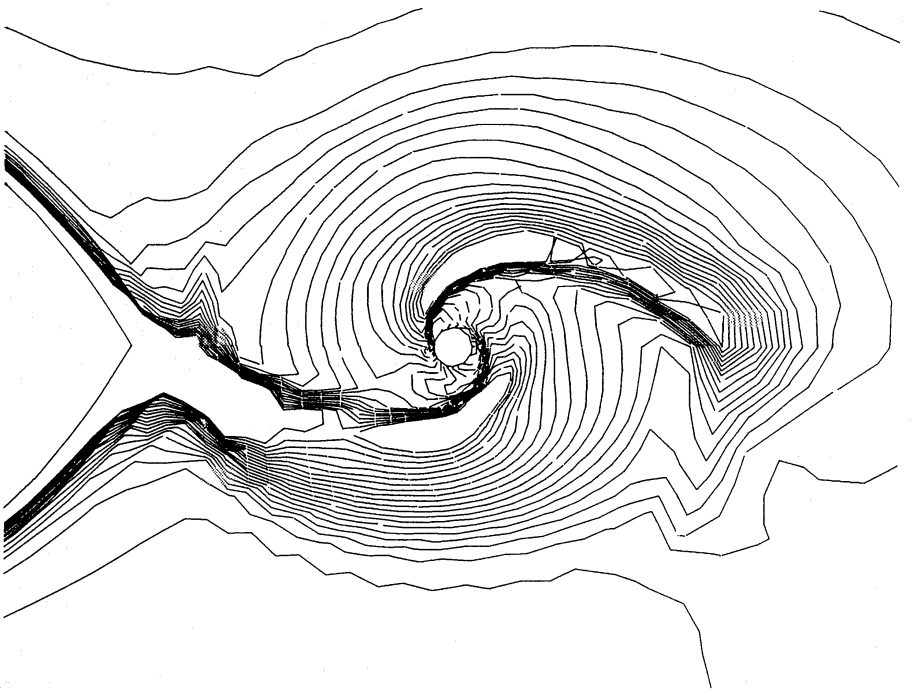

Figure 4. Density contours, ranging from 0.002 to 0.2, of the model with $c_0=0.15$ and $\gamma=1.2$.

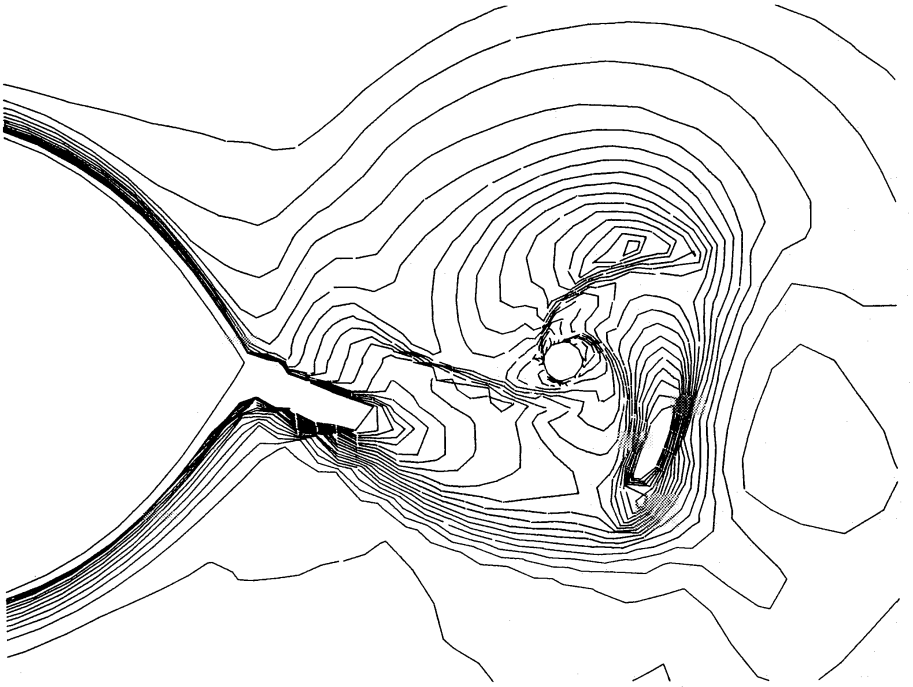

Figure 5. Density contours, ranging from 0.0005 to 0.03, of the model with $c_0=0.05$ and $\gamma=5/3$.

$A\Omega$ to be 100 km s^{-1}. Then $c_0=15$ km s^{-1} which gives $T=2\times10^4$ K. This may be rather high. Therefore we compute the case of $c_0=0.05$, which corresponds to $T=2500$ K.

In this case the density pattern is nearly the same as the higher c_0 cases, although the absolute value of the density is much smaller than in the other cases. An interesting feature is that there are sometimes three shocks on the accretion ring. Such a feature is also just visible in the cases of higher c_0. Fig. 5. shows the density distribution at the epoch, when three shocks are clearly seen. The shock strength oscillates with time, and there are stages when only two shocks are observable.

We also examined the case with $c_0=0.015$, but an instability stopped the second-order calculation. We then computed the same model using the first-order-accurate Osher scheme. The absolute value of the density is much lower than the higher c_0 case, but the density pattern (the elephant trunk and accretion ring) exist as well. As to the number of shocks, the first-order calculation does not give a reliable result, since a weak shock is smeared out.

3.4 THE CASE OF HOTTER GAS EMITTED FROM THE STAR

Next, we calculated the case of $c_0=0.5$ and $\gamma=5/3$. The temperature is very high in this case. However, as Fig. 6 shows, the flow pattern is still one of Roche lobe overflow. Shocks are present as well. When c_0 is increased to 1.0, we obtain a flow pattern of a stellar wind, which is quite different from the present Roche lobe overflow. A transition occurs between $c_0=0.5$ and $c_0=1.0$, and it will be studied in a separate paper.

3.5 MASS LOSS AND MASS ACCRETION

It is important to estimate the ratio of mass accretion onto the compact star to the total mass loss from the mass-losing star. Hensler (1982) estimated this value to be about 96 per cent. If this is the case, it results in a conservative evolution of binary systems.

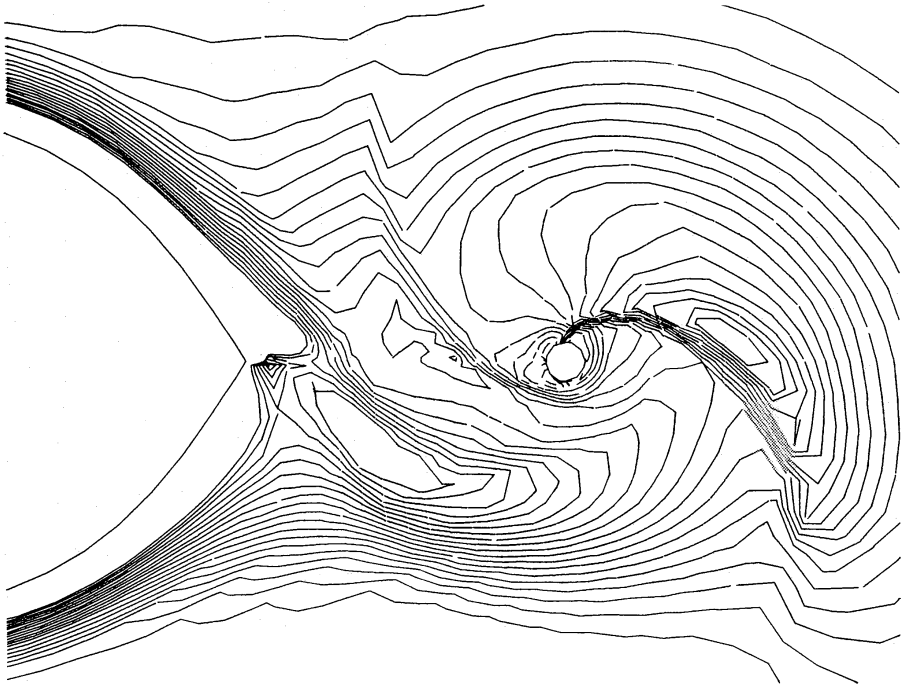

Figure 6. Density contours, ranging from 0.005 to 0.5, of the model with $c_0=0.5$ and $\gamma=5/3$.

In our calculations, this value is not constant with time but oscillates. This is because the mass loss rate from the mass-losing star is not kept constant but is regulated by circumstantial conditions as was discussed before. Fig. 7 shows the time evolution of the mass loss from the mass-losing star and the mass accretion on to the compact star in the model of cooler gas emitted. At the initial moment a very large fraction of gas is emitted from the mass-losing star into an almost vacuum surrounding. The mass accretion rate increases from zero to reach a steady value at about three-quarters of the revolution period. The mass loss rate oscillates around a mean value. It can be seen that about 60 per cent of the gas accretes on to the compact star.

This value depends on the parameters. In the model of hotter gas emitted, it is only about 20 per cent. Maximum accretion occurs for $c_0=0.15$ and $\gamma=1.2$, when it is as large as 90 per cent. This is probably because these shocks are the strongest among the cases studied in the present work.

An important question is what portion of the angular momentum loss is due to the shocks. This can be answered by increasing the number of meshes so as to reduce the amount of the numerical viscosity. We performed an experiment in which each mesh spacing in the radial direction is halved at $t=22$ in the model with $c_0=0.15$ and $\gamma=1.2$, and the subsequent evolution is followed to $t=27$.

It is found that the global density pattern is not altered except for a slight increase in the density in the accretion ring. An oscillation of the density pattern is excited at the transition epoch and it is not damped. The mass accretion rate also begins to oscillate. The average value of the mass accretion is reduced from 0.9 to 0.7 when the mesh spacing is halved.

On halving the mesh spacing, the numerical viscosity becomes one-quarter of the original value. In a standard axisymmetric accretion disc theory (see for example Pringle 1981), the mass accretion rate is proportional to the product of the viscosity and the surface density of the gas. If the mass accretion were entirely due to the shocks, the mass accretion rate would not be changed by this procedure. However, if the mass accretion were entirely due to the numerical viscosity, the mass accretion rate would become one-quarter of the original value, assuming the surface density to be the same. Considering these points, our result suggests that abouty 60–70 per cent of

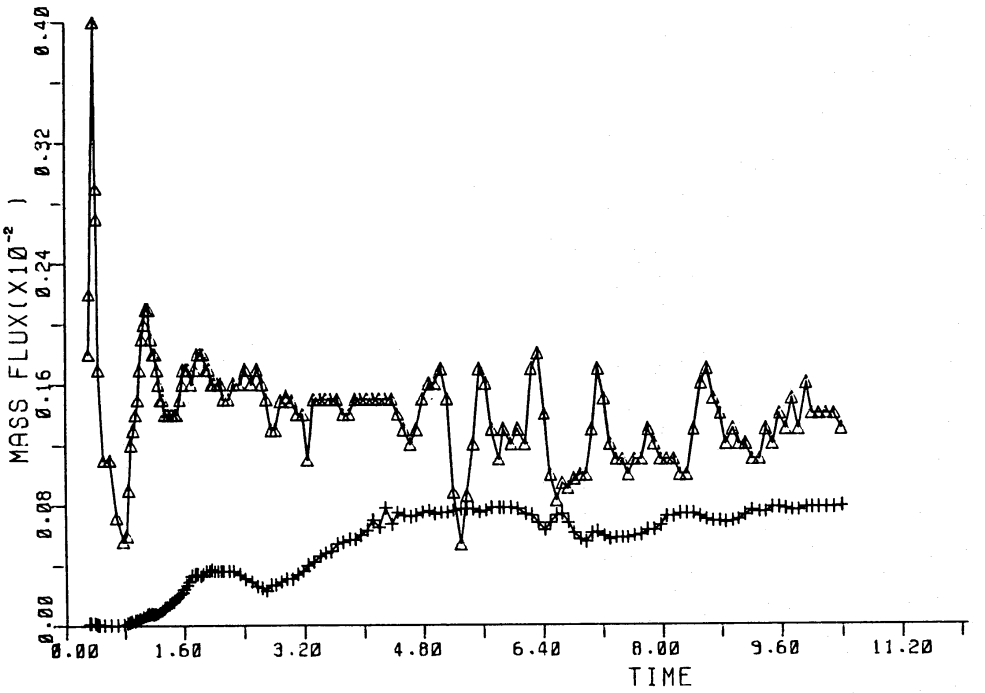

Figure 7. Time variation of the mass loss rate (triangles) and mass-accretion rate (crosses) in the model with $c_0=0.05$ and $\gamma=5/3$.

the total angular momentum loss is due to the shocks. Although the above considerations may not be complete, we can conclude that a fair amount of the mass accretion is due to the shocks.

The gas in the accretion disc is in a strongly shear motion and is highly supersonic. The high Reynolds' number has tempted workers to conclude that the flow must be highly turbulent. However, there is no justification for such an assertion, since the Rayleigh criterion for stability of the flow is amply satisfied (Safronov 1969). Therefore, if magnetic effects can be neglected, there may be a situation in which there is no viscosity present in the accretion disc except for an insignificant molecular viscosity.

Our numerical results pose an interesting possibility that the gas loses its angular momentum around the compact star even without turbulent and/or magnetic viscosity. However, further investigation is necessary before any definite conclusion can be reached. It is hoped to compute a gas flow around a compact star with a radius of say $0.01A$, using much finer numerical grids.

It is interesting to observe that the mass accretion rate is almost constant in spite of a varying mass loss rate (see Fig. 7). There are models to explain the time variation of the X-ray luminosity in terms of a varying mass loss rate induced by, say, changing the X-ray luminosity. However, such models will not work.

4 Conclusion

Two-dimensional hydrodynamic calculations of a flow of invisicid adiabatic gas in a semi-detached binary system are carried out using the second-order-accurate Osher scheme and a generalized curvilinear coordinate. The results are summarized as follows.

(1) Gas ejected from the surface of the mass-losing star flows through the L1 point and forms an elephant trunk. The flow is supersonic in the elephant trunk.

(2) The main part of the gas turns around the compact star to form an accretion ring.

(3) Two or three spiral-shaped shock waves are formed in the accretion ring because of the tidal force.

(4) After hitting the shock, gas loses its angular momentum around the compact star. The amount of angular momentum lost at the shock is larger than that due to the numerical viscosity. Therefore there is a possibility that the spiralling-in motion occurs even without turbulent and/or magnetic viscosity.

(5) Mass loss from the system occurs mainly through the L2 point.

(6) The mass loss rate from the mass-losing star oscillates with time, while the mass accretion rate is almost constant.

(7) The fraction of the gas accreted by the compact star depends on the parameters; it is generally in the range 20–90 per cent.

Acknowledgments

The computations have been performed on the Fujitsu VP100 vector processor and M382 at the Data Processing Center of Kyoto University, on M380 at the Institute of Space and Astronautical Science, and on M200 at the Nobeyama Radio Observatory. This research was supported by a Grant-in-Aid for Scientific Research (59540155) of the Ministry of Education, Science and Culture in Japan.

References

van Albada, G. D., van Leer, B. & Roberts, W. W., 1982. *Astr. Astrophys.*, **108,** 76.
Beam, R. M. & Warming, R. F., 1976. *J. Comp. Phys.*, **22,** 87.
Biermann, P., 1971. *Astr. Astrophys.*, **10,** 205.
Chakravarthy, S. & Osher, S., 1983. *AIAA J.*, **21,** 1241.
Flannery, B. P., 1975. *Astrophys. J.*, **201,** 661.
Godunov, S. K., 1959. *Mat. Sbornik,* **47,** 271.
Hensler, G., 1982. *Astr. Astrophys.*, **114,** 309; **114,** 319.
van Leer, B., 1984. *SIAM J. Sci. Stat. Comp.*, **5,** 1.
Lin, D. N. C. & Pringle, J. E., 1976. *Structure and Evolution of Close Binary Systems, IAU Symp. No. 73*, eds Eggleton, P. *et al.*, Reidel, Dordrecht, Holland.
Matsuda, T., 1981. *Prog. Theor. Phys. Suppl.*, **No. 70,** 249.
Osher, S. & Chakravarthy, S., 1983. *J. Comp. Phys.*, **50,** 447.
Pandolfi, M., 1984. *AIAA J.*, **22,** 602.
Prendergast, K. H., 1960. *Astrophys. J.*, **132,** 164.
Prendergast, K. H. & Taam, R. E., 1974. *Astrophys. J.*, **189,** 125.
Pringle, J. E., 1981. *Ann. Rev. Astr. Astrophys.*, **19,** 137.
Safronov, V. S., 1969. In *Evolution of the Earth and Planets*, Israel Program for Scientific Translations.
Sanders, R. H. & Huntley, J. M., 1976. *Astrophys. J.*, **209,** 53.
Sawada, K., Hachisu, I. & Matsuda, T., 1984.*Mon. Not. R. astr. Soc.*, **206,** 673.
Sorensen, S.-A., 1976. *Prog. Theor. Phys.*, **56,** 1484.
Sorensen, S.-A., Matsuda, T. & Fujimoto, M., 1976. *Astrophys. Space Sci.*, **43,** 491.
Sorensen, S.-A., Matsuda, T. & Sakurai, T., 1975. *Astrophys. Space Sci.*, **33,** 465.
White, N. E. & Mason, K. O., 1984. *18th ESLAB Symposium in Scheveningen*, Reidel, Dordrecht, Holland.

Appendix: Formulation and numerical scheme

A1 BASIC EQUATIONS

The basic equations describing a two-dimensional flow of perfect gas in a rotating frame of reference can be described in dimensionless form as (Sawada *et al.* 1984)

$$\mathbf{q}_t+\mathbf{F}_x+\mathbf{G}_y+\mathbf{H}=0, \tag{A1}$$

where

$$\mathbf{q}=\begin{pmatrix}\varrho\\ \varrho u\\ \varrho v\\ e\end{pmatrix},\quad \mathbf{F}=\begin{pmatrix}\varrho u\\ \varrho u^2+p\\ \varrho uv\\ (e+p)u\end{pmatrix},\quad \mathbf{G}=\begin{pmatrix}\varrho v\\ \varrho uv\\ \varrho v^2+p\\ (e+p)v\end{pmatrix},\quad \mathbf{H}=\begin{pmatrix}0\\ \varrho k_x\\ \varrho k_y\\ \varrho(uk_x+vk_y)\end{pmatrix}, \tag{A2}$$

where ϱ, u, v, e, p, k_x and k_y are the density, the x and y components of the velocity, the total energy per unit volume, the pressure and the x and y components of the force, respectively.

The x and y components of the force are

$$k_x=-2v-x+\frac{\zeta}{1+\zeta}\frac{x_1}{r_1^3}+\frac{1}{1+\zeta}\frac{x_2}{r_2^3},$$

$$k_y=2u-y+\frac{\zeta}{1+\zeta}\frac{y_1}{r_1^3}+\frac{1}{1+\zeta}\frac{y_2}{r_2^3}. \tag{A3}$$

Here, ζ is the mass ratio and is set to be unity in the present work, r_i $(i=1, 2)$ is the distance from the point considered to the centre of the respective star, and x_i and y_i are its Cartesian components.

The equation of state is

$$p=(\gamma-1)\{e-\tfrac{1}{2}\varrho(u^2+v^2)\}. \tag{A4}$$

Under a general coordinate transformation of the form

$$\xi=\xi(x, y),$$

$$\eta=\eta(x,y), \tag{A5}$$

equation (A1) can be written in the strong conservation form as

$$\hat{\mathbf{q}}_t+\hat{\mathbf{F}}_\xi+\hat{\mathbf{G}}_\eta+\hat{\mathbf{H}}=0, \tag{A6}$$

where

$$\hat{\mathbf{q}}=\frac{1}{J}\begin{pmatrix}\varrho\\ \varrho u\\ \varrho v\\ e\end{pmatrix},\quad \hat{\mathbf{F}}=\frac{1}{J}\begin{pmatrix}\varrho\hat{U}\\ \varrho u\hat{U}+\xi_x p\\ \varrho v\hat{U}+\xi_y p\\ (e+p)\hat{U}\end{pmatrix},\quad \hat{\mathbf{G}}=\frac{1}{J}\begin{pmatrix}\varrho\hat{V}\\ \varrho u\hat{V}+\eta_x p\\ \varrho v\hat{V}+\eta_y p\\ (e+p)\hat{V}\end{pmatrix},\quad \hat{\mathbf{H}}=\frac{1}{J}\begin{pmatrix}0\\ \varrho k_x\\ \varrho k_y\\ \varrho(uk_x+vk_y)\end{pmatrix}. \tag{A7}$$

In the above expressions, J is the transformation Jacobian and $\hat{U}$ and $\hat{V}$ are the contravariant velocities defined as

$$J=\xi_x\eta_y-\xi_y\eta_x,$$

$$\hat{U}=u\xi_x+v\xi_y,$$

$$\hat{V}=u\eta_x+v\eta_y. \tag{A8}$$

A2 OSHER SCHEME

The basic equations described above are solved by the second-order-accurate version of the Osher upwind finite difference scheme (Osher & Chakravarthy 1983; Chakravarthy & Osher

1983). In ordinary aerodynamic problems, the most widely used method would probably be the Beam & Warming implicit scheme (Beam & Warming 1976), which has second-order accuracy in space compared with the first-order accuracy of the original Osher scheme.

We used the Beam & Warming scheme to compute the flow in a contact binary system (Sawada *et al.* 1984). However, in the present problem, the topology of the system is triply connected, and we need two cuts in space to map the physical plane on to a singly connected computational plane. It is not easy to handle the periodicity condition on the cuts in implicit schemes. Therefore, we apply an explicit scheme.

Among various explicit schemes, the Godunov scheme (Godunov 1959; see van Albada *et al.* 1982 for its detail) and the Osher scheme are known to be very robust. They do not show wiggles, which are characteristic of most higher-order schemes such as the Lax–Wendroff scheme and the MacCormack scheme, near discontinuities. The former schemes can handle very strong shocks and very sharp pressure contrast stably. The Osher scheme can be considered as a simplified version of the Godunov scheme (van Leer 1984), and is suited to coding for vector processors. Therefore we used the Osher scheme in the present work.

The original Osher scheme is of first-order accuracy in space. We performed computations of the gas flow in the present model using the first-order scheme. We found that the method was not completely satisfactory because spurious entropy production was not negligible. Therefore, we found only one spiral shock in the accretion disc compared with two or three in the second-order-accurate scheme.

Here we explain the first-order version in physical terms. Consider a one-dimensional Euler equation written in a conservation form

$$u_t + F_x = 0,$$

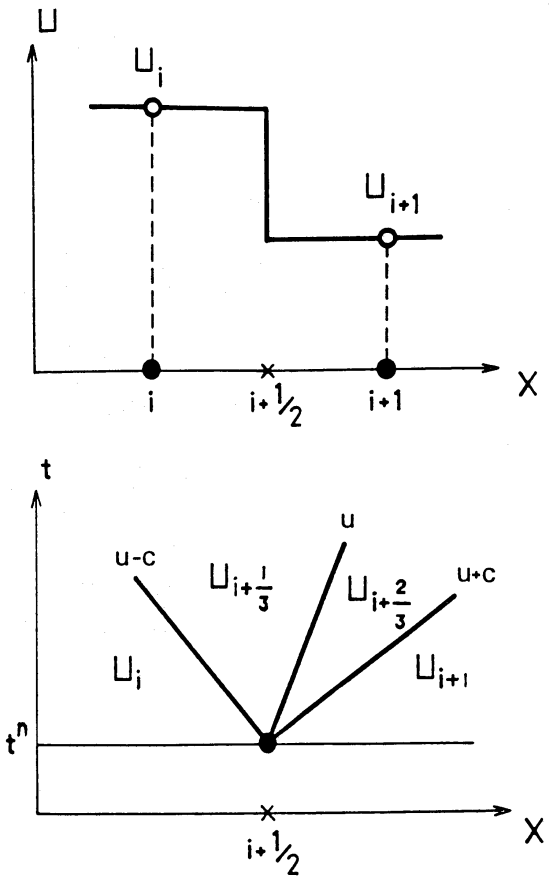

Figure A1. Illustration of the Riemann problem used in the Osher scheme.

which can be discretized as follows:

$$\frac{u_i^{n+1}-u_i^n}{\Delta t}+\frac{F_{i+1/2}^n-F_{i-1/2}^n}{\Delta x}=0.$$

The problem is how to evaluate the flux $F_i+_{1/2}$ at the intermediate position $x_{i+1/2}$. In a conventional central difference scheme, it would be evaluated as $F_{i+1/2}=F\{\frac{1}{2}(u_i+u_{i+1})\}$. Such a scheme is known to be unstable.

There is a more sophisticated way. Let us model the flow at time t^n by a uniform flow u_i in the first half-interval $(x_i, x_{i+1/2})$ and a uniform flow u_{i+1} in the second half-interval $(x_{i+1/2}, x_{i+1})$. A discontinuity located at the midpoint $x_{i+1/2}$ separates the two half-intervals. Such a configuration is called a piecewise constant configuration.

Let us consider the evolution of this configuration. This is called a Riemann problem. The exact solution of the Riemann problem involves a computational effort with iterative procedures and does not suit vector processors. Instead of solving the Riemann problem exactly, Osher approximated the shock by a simple wave and solved the problem analytically.

In this approximation, three characteristic waves corresponding to three eigenvalues $u-c$, u and $u+c$, where c is the speed of sound, emerge as shown in Fig. A1. Note that the arrangement of these three characteristic waves is different from the original Osher scheme and is due to Pandolfi (1984). The waves $u-c$ and $u+c$ approximate either a shock wave or an expansion wave, while the wave u is the contact surface. The interaction between the two uniform regions u_i and u_{i+1} generates two further uniform regions $u_{i+1/3}$ and $u_{i+2/3}$. In the case shown in Fig. A1, where the waves $u+c$ and u propagate to the right, while $u-c$, propagates to the left, the flux at the midpoint may be evaluated from $u_{i+1/3}$. The algorithm employed in the Osher scheme is a little more involved if sonic points exist in the region.

We make the algorithm accurate to second-order using a technique proposed by van Albada *et al.* (1982). The detail of our algorithm and the test calculations will be published elsewhere and are available from the authors.

A3 BOUNDARY CONDITIONS AND AN INITIAL CONDITION

The boundary condition at the surface of the mass-losing star was discussed earlier, but let us explain it in more detail. Note that our algorithm to treat the boundary condition is different from Osher's (Osher & Chakravarthy 1983). Let us consider the one-dimensional case. At a point x_0 just inside the surface of the star, all components of $\mathbf{q}_0$ are specified. Since $\mathbf{q}_1$ is known in the computation, we can solve the Riemann problem between these two states to decide the intermediate values $\mathbf{q}_{1/3}$ and $\mathbf{q}_{2/3}$.

In a supersonic outflow condition, all characteristic waves run right (outwards). In this case $\mathbf{q}_0$ will be chosen as the boundary value. If waves travel as is shown in Fig. A1, which is our subsonic outflow case, $\mathbf{q}_{1/3}$ should be used as the boundary value. Therefore the boundary value just on the surface cannot be known *a priori*. It is controlled by the condition just outside the surface. The mass loss rate is therefore not kept constant, as can be seen in the preceding results.